

NH⁺–F Hydrogen Bonding in a Fluorinated “Proton Sponge” Derivative: Integration of Solution, Solid-State, Gas-Phase, and Computational Studies

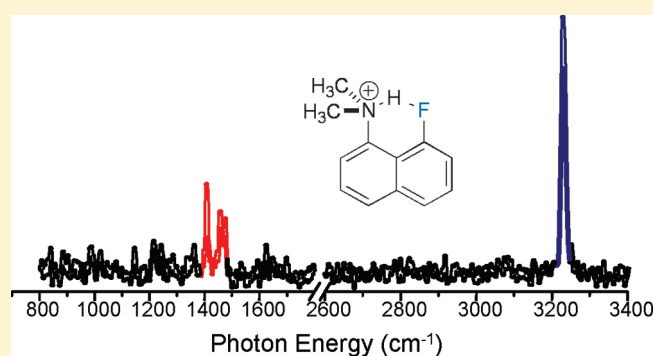
Michael T. Scerba,[†] Christopher M. Leavitt,[‡] Matthew E. Diener,[†] Andrew F. DeBlase,[‡] Timothy L. Guasco,[‡] Maxime A. Siegler,[†] Nathaniel Bair,[†] Mark A. Johnson,^{*,‡} and Thomas Lectka^{*,†}

[†]Department of Chemistry, New Chemistry Building, Johns Hopkins University, 3400 North Charles Street, Baltimore, Maryland 21218, United States

[‡]Department of Chemistry, Yale University, P.O. Box 208107, New Haven, Connecticut 06520, United States

S Supporting Information

ABSTRACT: We report detailed studies on the characterization of an intramolecular NH–F hydrogen bond formed within a fluorinated “proton sponge” derivative. An ammonium ion, generated from 8-fluoro-*N,N*-dimethylnaphthalen-1-amine, serves as a charged hydrogen bond donor to a covalently bound fluorine appropriately positioned on the naphthalene skeleton. Potentiometric titrations of various *N,N*-dimethylnaphthalen-1-amines demonstrate a significant increase in basicity when hydrogen bonding is possible. X-ray crystallography reveals that NH–F hydrogen bonding in protonated 8-fluoro-*N,N*-dimethylnaphthalen-1-amine is heavily influenced by ion pairing in the solid state; bifurcated and trifurcated hydrogen bonds are formed depending on the counterion utilized. Compelling evidence of hydrogen bonding in the 8-fluoro-*N,N*-dimethylnaphthyl-1-ammonium cation is provided by gas-phase cryogenic vibrational photodissociation spectroscopy. Solution-phase infrared spectroscopy provides complementary results, and the frequencies of the N–H stretching mode in both phases are in excellent agreement with the computed vibrational spectra. NMR analysis of protonated 8-fluoro-*N,N*-dimethylnaphthalen-1-amine demonstrates significant H–F coupling between the N–H hydrogen and fluorine that cannot be attributed to long-range, through-bond interactions; the couplings correlate favorably with calculated values. The results obtained from these experiments are congruent with the formation of an NH–F hydrogen bond upon protonation of 8-fluoro-*N,N*-dimethylnaphthalen-1-amine.



INTRODUCTION

Hydrogen bonding is known to play a critical role in several facets of enzyme biochemistry including substrate recognition, catalytic activity, and protein structure.¹ The recent surge in the number of fluorinated biochemicals and pharmaceuticals has led to substantial interest in the interactions of substrate-bound fluorine atoms with enzymatic hydrogen bond donors. A recent and thorough investigation of the Protein Data Bank revealed a significant number of proposed OH–F and NH–F contacts between various enzymes and fluorinated substrates.² For example, neutral OH–F hydrogen bonds have been reported within aldol reductases,³ while similar NH–F contacts are implicated in the inhibition of glucanase⁴ and glycerol kinase.⁵ Perhaps even more intriguing is the prospect of a *charged* donor interacting with a neutral fluorinated organic acceptor (Figure 1). It has been stated that putative charged hydrogen bonding can increase the binding affinity of certain drugs 3000-fold while corresponding neutral–neutral interactions contribute a modest 15-fold increase.⁶ Charged NH⁺–F interactions have been proposed



Figure 1. Hydrogen bonding interactions of fluorine with charged N-donors in biological systems.

for a variety of fluorinated substrates bound with elastase,⁷ HMG-CoA reductase,⁸ xylanase,⁹ and nucleotide diphosphate kinase.¹⁰

Despite the numerous conjectures of biochemically relevant NH–F hydrogen bonding, the presence of these contacts in biological systems is justified primarily by the proximity of the hydrogen bonding partners within crystal structures. Ironically, thorough investigations of the intimate association of *charged* hydrogen bond donors with fluorinated organic molecules are virtually undocumented to date despite intriguing reports of

Received: July 23, 2011

Published: September 02, 2011

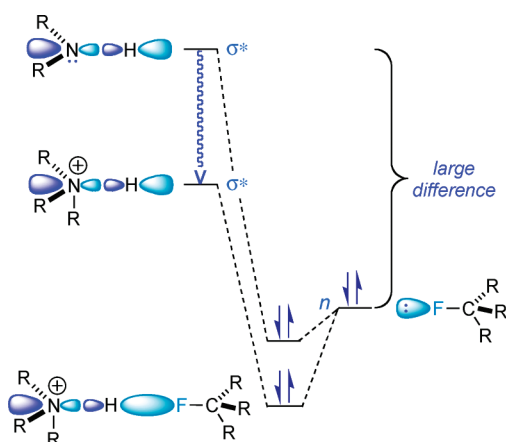


Figure 2. Orbital diagram for NH^+-F hydrogen bonding.

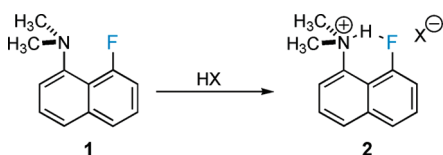


Figure 3. Formation of an NH^+-F hydrogen bond.

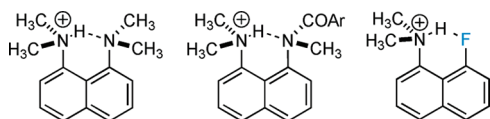


Figure 4. 1,8-Disubstituted "peri" naphthalenes demonstrating significant hydrogen bonds.

neutral $\text{C}-\text{F}\cdots\text{H}-\text{O}^{11}$ and $\text{C}-\text{F}\cdots\text{H}-\text{N}^{12}$ bonding in a variety of organic substrates. In the case of charged NH^+-F hydrogen bonding, one can imagine the marked stabilization afforded by the interaction of a filled fluorine n orbital with an empty σ^* orbital of a charged tertiary ammonium ion hydrogen bond donor (Figure 2). The σ^* fragment orbital of the ammonium species is lower in energy than that of the corresponding amine and produces superior stabilization.

We felt that a 1,8-disubstituted naphthalene derivative would provide the ideal framework on which to document conclusive hydrogen bonding between a charged NH^+ and covalently bound fluorine (Figure 3). It has been shown numerous times that 1,8-bis(dimethylamino)naphthalenes are attractive substrates for investigating hydrogen bonding between the spatially proximate "peri" positions and often provide unambiguous evidence for charged $\text{N}-\text{H}\cdots\text{N}$ hydrogen bonds in many instances (Figure 4).¹³ Unfortunately, the detailed study of positively charged donors to fluorine in model systems is especially complicated by the competitive presence of counterions and potential hydrogen bond bifurcation that may sap the strength of the interaction of interest. In this paper, we detail solution-phase, gas-phase, and solid-state studies of an intramolecularly bound system containing a charged NH^+-F hydrogen bond.

RESULTS AND DISCUSSION

Effects of Hydrogen Bonding on Relative Basicity. Precise measurements of hydrogen bond strength are fraught with

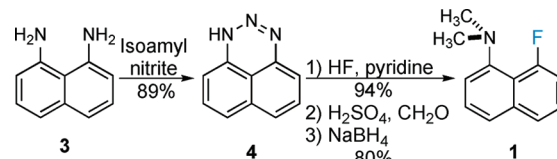


Figure 5. Synthesis of 8-fluoro-*N,N*-dimethylnaphthalen-1-amine.

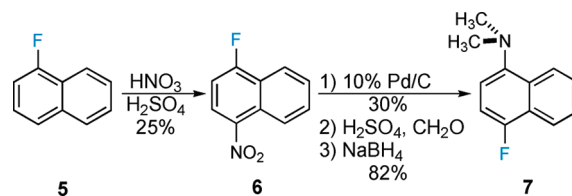


Figure 6. Synthesis of 4-fluoro-*N,N*-dimethylnaphthalen-1-amine.

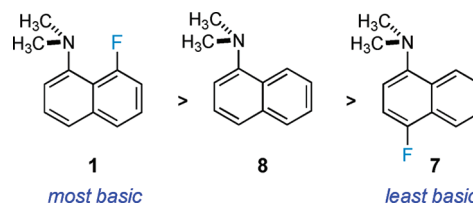


Figure 7. Predicted trend in relative basicity.

uncertainty and are critically reliant on the nature of comparative model systems. Nevertheless, an initial, grossly qualitative measure of hydrogen bond strength could be deduced by an evaluation of the basicity of **1** relative to appropriate controls. As such, 8-fluoro-*N,N*-dimethylnaphthalen-1-amine **1** was synthesized in 66% overall yield, starting from commercially available 1,8-diaminonaphthalene **3** (Figure 5).^{14,15} Isomeric 4-fluoro-*N,N*-dimethylnaphthalen-1-amine **7** was synthesized by nitration of 1-fluoronaphthalene,¹⁶ subsequent hydrogenation,¹⁷ and finally reductive dimethylation (Figure 6).

If hydrogen bonding were present in protonated 8-fluoro-*N,N*-dimethylnaphthalen-1-amine **1**, fluorine should act to stabilize the conjugate acid by acting as a hydrogen bond acceptor; the basicity of **1** should be greater than that of nonfluorinated *N,N*-dimethylnaphthalen-1-amine **8** and isomeric 4-fluoro-*N,N*-dimethylnaphthalen-1-amine **7** (Figure 7). On the other hand, in the absence of hydrogen bonding, the basicity trend should be reversed, correlating closely with electronic effects.¹⁸ In either case, steric effects should not influence the basicity trends because of the grossly similar van der Waals radii of fluorine and hydrogen (1.47 Å and 1.20 Å, respectively).¹⁹ Therefore, a sequence of simple titrations was designed to elucidate the effect that hydrogen bonding exerts on the relative basicities of a series of *N,N*-dimethylaminonaphthalene derivatives.

Careful consideration of the solvent medium was necessary, as solvation could, of course, greatly affect the basicity measurements. Nitromethane was chosen because of its large dielectric constant, weak acidity, and ability to dissolve both the substrates and acid titrants. In addition, particular care was given to the choice of acid titrant. Perchloric acid was selected because of its strength, its weakly hydrogen-bond-accepting conjugate base,²⁰ and its successful use in titrations of similar amines.²¹

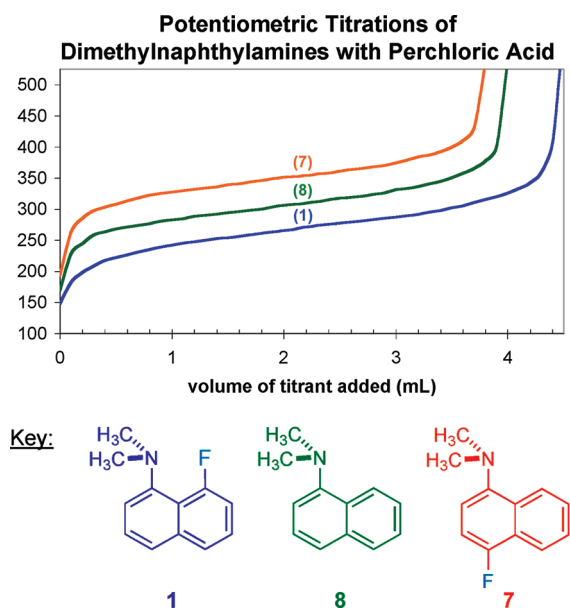


Figure 8. Potentiometric titration curves.

Figure 8 shows an overlay of the titration curves obtained from triplicate runs of each substrate. The derived $E_{1/2}$ values are used as a relative gauge of basicity.²² It is clear that 8-fluoro-*N,N*-dimethylnaphthalen-1-amine **1** is the most basic of all the naphthylamines tested, with an average $E_{1/2}$ 31 mV lower than that of *N,N*-dimethylnaphthalen-1-amine **8**, and 86 mV lower than that of 4-fluoro-*N,N*-dimethylnaphthalen-1-amine **7**. When these values were analyzed using the method developed by Streuli,²² a 10-fold increase in basicity of **1** relative to **7** was realized. This considerable difference suggests that simple electronic effects (which predict the opposite progression) are not responsible for the observed trend in basicity. Therefore, conjugate acid stabilization arising from intramolecular NH–F hydrogen bonding is entirely plausible and has direct influence over the basicities of the *N,N*-dimethylnaphthalen-1-amines tested. Finally, one can expect that in solvents less coordinating than that of nitromethane, this basicity difference would increase.

Computational Studies. We believed that some simple density functional theory (DFT) calculations could provide further qualitative information regarding the nature of the hydrogen bond.²³ If hydrogen bonding were possible in 8-fluoro-*N,N*-dimethylnaphthalen-1-amine **1**, isodesmic proton transfer from an isomeric fluoro-*N,N*-dimethylnaphthyl ammonium ion would be favorable because of conjugate acid stabilization. At the same time, inductive effects that occur in systems incapable of intramolecular hydrogen bonding would not be prevalent. The relief of strain upon protonation should be minimal (as compared to classical proton sponges).²⁴ The reactions shown below were analyzed using the DFT/B3LYP functional at the 6-311+G** level of theory. Proton transfer from **9** to **1** is predicted to be exothermic by 7.64 kcal/mol due primarily to the hydrogen bond formed in **10** upon protonation (Figure 9, reaction a).

Investigation of the effects of fluorine substitution on anilinium ion basicity (a system incapable of intramolecular hydrogen bonding) demonstrated that proton transfer from **11** to **12** was exothermic by 2.19 kcal/mol and consistent with the trend in electronic substituent effects (Figure 9, reaction b). While this

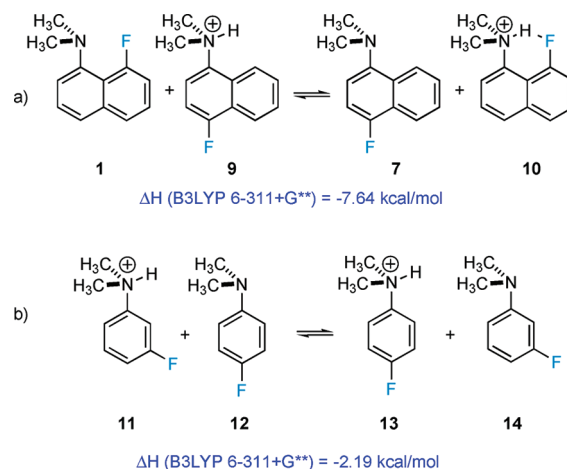


Figure 9. Isodesmic proton transfer between (a) isomeric fluoro-naphthalenes and (b) isomeric fluoroanilines.

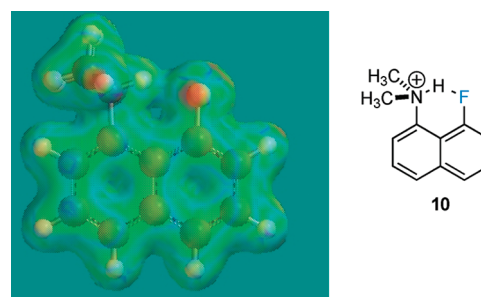


Figure 10. Electron density map of ion **10**, optimized at DFT/B3LYP/6-311+G**.

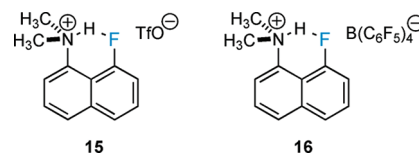


Figure 11. 8-Fluoro-*N,N*-dimethylnaphthalen-1-amine salts.

result is not surprising, it serves to show that a *meta*-fluorine exerts a considerable acidifying effect on dimethylanilinium ions. Compound **10** contains fluorine in a “*meta*-like” position, yet does not follow a similar trend in acidity. Thus, it is quite likely that calculations may underestimate the precise degree of hydrogen bonding in this system and further illustrate the complexity in quantifying hydrogen bond interactions.

A simple electrostatic potential map provides additional qualitative evidence in favor of NH–F hydrogen bonding. The space-filling model below demonstrates the classic six-membered ring motif characteristic of numerous protonated proton sponge derivatives and clearly shows the charged donor-neutral acceptor interaction (Figure 10). A significant amount of electron density is predicted between the ammonium hydrogen and the aryl fluorine, suggesting that appreciable hydrogen bonding occurs in protonated 8-fluoro-*N,N*-dimethylnaphthalen-1-amine.

X-ray Crystallography. We then turned our attention to obtaining crystals of protonated 8-fluoro-*N,N*-dimethylnaphthalen-1-amines suitable for X-ray structure determination (Figure 11).

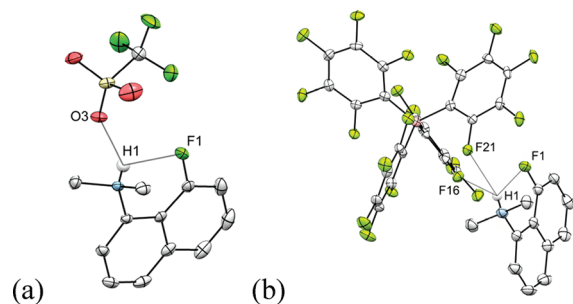


Figure 12. Displacement ellipsoid plots (50% probability level) of (a) 8-fluoro-*N,N*-dimethylnaphthalen-1-ammonium triflate **15** and (b) 8-fluoro-*N,N*-dimethylnaphthalen-1-ammonium BARF **16** highlighting the bifurcated and trifurcated hydrogen bonds, respectively. Nonessential hydrogens were omitted for clarity. Selected bond distances and angles: (a) $H1 \cdots F1 = 2.131(18)$ Å, $H1 \cdots O3 = 2.148(19)$ Å, $N1-H1-F1 = 120.7(15)^\circ$, $N1-H1-O3 = 145.0(16)^\circ$. (b) $H1 \cdots F1 = 2.027(17)$ Å, $H1 \cdots F16 = 2.339(16)$ Å, $H1 \cdots F21 = 2.471(16)$ Å, $N1-H1-F1 = 129.6(14)^\circ$, $N1-H1-F16 = 140.5(14)^\circ$, $N1-H1-F21 = 121.8(14)^\circ$.

Compound **1** was protonated with triflic acid (HOTf) in CH_2Cl_2 , and analysis of the resulting crystalline salt **15** revealed the presence of a nearly symmetrical, bifurcated hydrogen bond between one of the three triflate oxygens and the aryl fluoride. The associated D–H–A angles (D = donor atom, A = acceptor atom) are also consistent with hydrogen bond bifurcation (Figure 12, structure a); strong, nonbifurcated systems typically feature angles in the range of 165 – 180° .²⁵ This phenomenon is supported by plotting contoured difference Fourier maps that clearly depict bifurcation of the ammonium hydrogen between the fluoronaphthalene system and one triflate oxygen. (Figure 13, map a). Such a result is not terribly surprising, as triflate is known to be an excellent hydrogen bond acceptor.²⁶ The presence of a bifurcated hydrogen bond “sapping” the strength of the desired interaction prompted investigation of less coordinating counterions.

Protonation of 8-fluoro-*N,N*-dimethylnaphthalen-1-amine **1** was achieved in CH_2Cl_2 using $HCl(g)$, and the chloride ion was exchanged for the BARF ion²⁷ (Figure 11). Single crystal X-ray structure determination of the resulting salt revealed an interesting trifurcated hydrogen bond including two unexpected contacts of the ammonium hydrogen with fluorine atoms of the BARF counterion (Figure 12, structure b). Both of these contacts, however, are considerably longer than the $H1-O3$ contact formed in the triflate salt and suggest a much weaker coordination of the BARF counterion relative to the triflate analogue. Contoured difference Fourier mapping also supports a trifurcated bond and suggests that the ammonium hydrogen resides in closer relative contact to the naphthyl fluorine as compared to the triflate species (Figure 13, map b).

The nature of charged species is such that one cannot reasonably expect complete noncoordination of the ionic partners, especially when associations occur within the rigid, ordered framework of a crystal lattice. Charged hydrogen bonds are particularly susceptible to these forces.²⁸ We noted that our triflate and BARF structures (**15** and **16**, respectively) featured $NH-F$ contacts that distort out of plane with respect to the naphthalene ring system (Figure 14). In the case of the triflate salt, analysis of the $C10-C1-N1-H1$ torsional angle reveals an approximate 39.5° deviation from planarity. However, when BARF is exchanged for triflate, a 29.5° difference is observed,

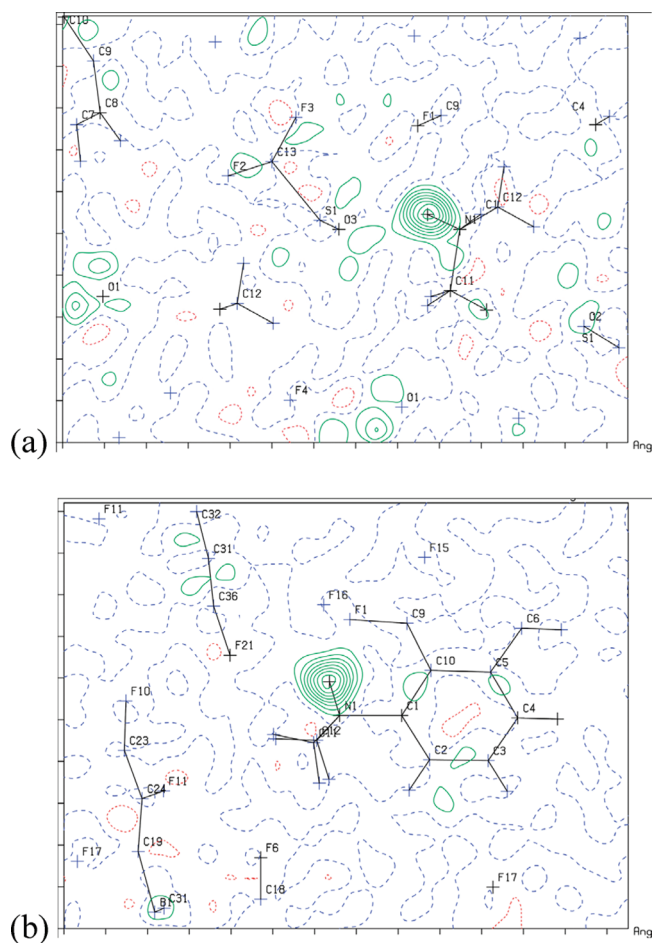


Figure 13. Contoured difference Fourier maps of (a) 8-fluoro-*N,N*-dimethylnaphthalen-1-ammonium triflate **15** with respect to the $N1-F1-O3$ plane and (b) 8-fluoro-*N,N*-dimethylnaphthalen-1-ammonium BARF **16** with respect to the $C1-N1-H1$ plane. Prior to the difference Fourier map calculations, the $H1$ atom was omitted so that its position is derived by locating the residual electron density.

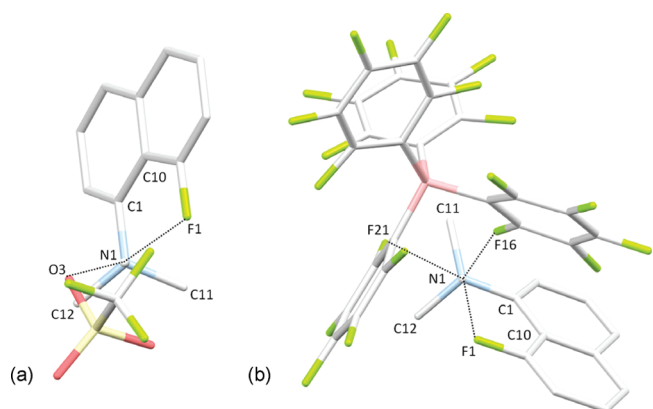


Figure 14. Projections showing the $N-H \cdots A$ ($A = O, F$) contacts for (a) triflate salt **15** and (b) BARF salt **16** as viewed down the $N1-H1$ bond to the mean plane $C1-C11-C12$. Selected $N \cdots A$ distances; for (a) $N1 \cdots O3 = 2.8867(17)$ Å, $N1 \cdots F1 = 2.6676(16)$ Å. (b) $N1 \cdots F1 = 2.6466(16)$ Å, $N1 \cdots F16 = 3.0396(16)$ Å, $N1 \cdots F21 = 3.0033(16)$ Å.

demonstrating a significant flattening of the $CF-HN$ contact and suggesting an increase in the degree of hydrogen bonding. In

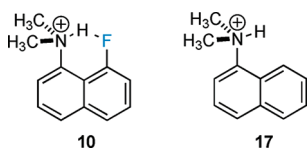


Figure 15. Ions examined by cryogenic infrared photodissociation spectroscopy.

contrast, the stronger hydrogen bonds found in classical proton sponges are often less sensitive to crystal packing pressures and the coordinating effects of counterions; in a variety of cases, the N–H–N bond resides in the plane of the naphthalene skeleton.²⁹

While it is possible that neutron diffraction may provide a more accurate determination of the position of the ammonium hydrogen along the N–H bond,³⁰ we reason that because we observe considerable counterion coordination in the solid state, such studies will not yield considerably more information than we already possess. The torsional angle should not deviate appreciably; the tetrahedral geometry of the ammonium ion (and therefore the directional vector of the N–H bond) is dictated by the dimethylaminonaphthalene system, not the diffraction technique. In addition, trends concomitant with a move toward less coordinating counterions suggest hydrogen bonding occurs in the solid state to a degree that is heavily dictated by intermolecular forces. Ultimately, the NH–F hydrogen bond will never be as short or as planar as theory predicts unless the effects of counterions are completely eliminated.

Initial Infrared Spectroscopic Analysis. After the results of the crystallographic analyses demonstrated the appreciable influence of the counterion, we wondered how NH–F hydrogen bonding would be affected by *elimination* of the interactions entirely. An initial DFT/B3LYP/6-311+G** analysis of a series of protonated *N,N*-dimethylaminonaphthyl-1-amines and fluorinated analogues revealed that strategic incorporation of fluorine into the 8-position was predicted to show an N–H stretching absorbance at 3262 cm⁻¹, red-shifted 66 cm⁻¹ relative to the unfluorinated compound in the absence of solvent or counterion effects. Such a result seems intuitive; one can imagine an appreciable weakening of the N–H bond resulting from intramolecular hydrogen bonding. In fact, a pronounced bathochromic shift in X–H stretching mode is often characteristic of compounds that engage in hydrogen bonding.³¹

Gas-Phase Studies. Investigating ions in the gas phase³² is particularly attractive because the complications arising from counterions or solvent interactions can be eliminated. Infrared spectroscopy provides a direct probe of molecular structure, and recent advances in gas-phase IR techniques have illustrated that spectra can be greatly improved when ions are cooled to cryogenic temperatures.³³ By measuring the systematic shift on the N–H⁺ stretch of the 8-fluoro-*N,N*-dimethylnaphthyl-1-ammonium cation versus the *N,N*-dimethylnaphthyl-1-ammonium ion, **10** and **17** (Figure 15), respectively, the extent of NH⁺–F hydrogen bonding can be empirically measured.

The gas-phase cryogenic vibrational photodissociation spectra over the 2600–3600 cm⁻¹ range are presented in Figure 16a and 16b for ions **10** and **17**, respectively. For both ions, an intense transition is identified as the N–H stretch of the protonated amine with the observed band in the spectrum of **10**, located at 3228 cm⁻¹, red-shifted by ~35 cm⁻¹ from the analogous transition in the spectrum of **17**. The scaled harmonic frequency

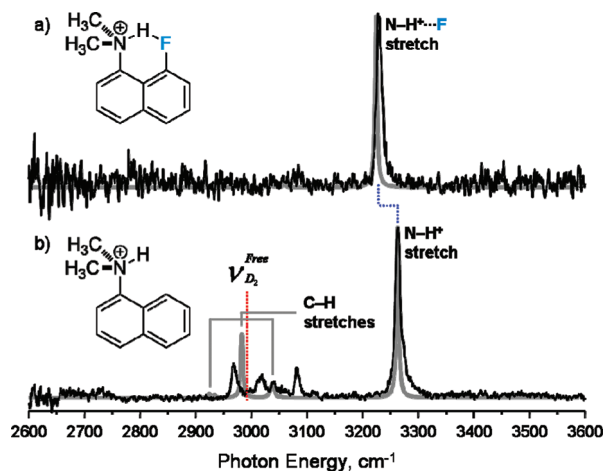


Figure 16. Gas-phase cryogenic vibrational photodissociation spectra over the 2600–3600 cm⁻¹ photon energy range of (a) 8-fluoro-*N,N*-dimethylnaphthyl-1-ammonium cation **10** tagged with two H₂ molecules and (b) *N,N*-dimethylnaphthyl-1-ammonium cation **17** tagged with a single D₂. In both cases, the vibrational spectra were obtained by monitoring the photoproduction of the bare ammonium cation. The analogous harmonic frequency spectra (MP2/6-311+G**) are overlaid in gray and were scaled by 0.943 to bring the calculated N–H stretch for **17** into agreement with the experimentally measured band position.

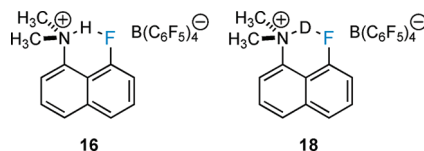


Figure 17. Protonated and deuterated H-bonding substrates.

spectra (MP2/6-311+G**) are overlaid (gray trace) on top of the experimental vibrational spectra in Figure 16, and the N–H stretching fundamentals are in good agreement with the experimentally measured band positions, with a calculated red shift of 39 cm⁻¹ between ions **10** and **17**. The observed red shift corresponds to a lengthening of N–H bond by ~0.0017 Å in the fluorinated analogue based on the electronic structure calculations. The most striking difference in the optimized geometry between **10** and **17** is the C10–C1–N1–H1 torsional angle, which is nearly planar in **10** (2.301°), while in **17** this angle increases to 21.754°, giving some indication of a favorable intramolecular interaction between the proton and the fluorine.

A series of bands in the 2950–3100 cm⁻¹ energy range are observed in the spectrum of **17** (Figure 16b), which are derived from the C–H stretches on the aromatic and methyl groups, with the C8–H stretch of the naphthalene ring calculated to carry significant intensity. A transition centered at 2968 cm⁻¹ is assigned to the perturbed D₂ stretch, shifted ~20 cm⁻¹ from the forbidden IR transition of the free molecule. The molecular tag is thought to be localized around the charge center, and previous studies on molecules containing protonated amines^{33c} indicate that D₂ binds perpendicular with respect to the N–H⁺ bond in a t-shape arrangement. It is important to note that a band located at 4120 cm⁻¹ was observed in the spectrum of **10**, which was taken using H₂ as a tag, that is ~40 cm⁻¹ below the unperturbed H₂ stretch. Thus, the tags appear to be minimally invasive mass “messengers” that allow access to the structures of the isolated ions.

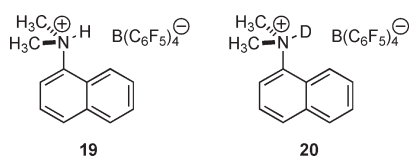


Figure 18. Protonated and deuterated substrates incapable of intramolecular H-bonding.

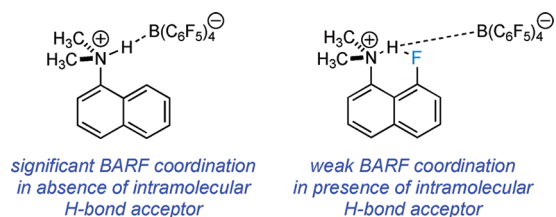


Figure 19. Effect of intramolecular hydrogen bonding on counterion coordination.

Solution Studies. With these results in hand, we wondered how the hydrogen bond would be affected in solution once the effects of solvation and counterions were introduced. When BARF salt **16** was dissolved in dichloromethane, a prominent N–H absorbance was detected at 3242 cm^{−1}, in good agreement with both the theoretical value and the cryogenic ion data (3228 cm^{−1}). When the key hydrogen was exchanged for deuterium (Figure 17), a weak but sharp peak was observed at 2411 cm^{−1}, again in excellent agreement with the calculated value of 2399 cm^{−1}. The $\nu_{\text{NH}}/\nu_{\text{ND}}$ ratio of 1.34 is consistent with a double minimum potential, high barrier hydrogen bond. Similar isotopic vibrational ratios are obtained for six-membered intramolecular hydrogen bonds formed from phenolic trisubstituted Mannich bases dissolved in dichloromethane.³⁴

However, when we investigated the corresponding nonfluorinated control compounds **19** and **20** (Figure 18), the desired N–H peaks were too weak to be observed, or deviated significantly from the predicted values. While we were initially puzzled by this result, we reasoned that appreciable hydrogen bonding between the BARF counterion and the ammonium N–H hydrogen had to be occurring in the absence of a suitable intramolecular hydrogen bond acceptor (Figure 19). Such results are not without precedent; studies performed by Sweigart and Son on charge-assisted hydrogen bonding in ionic rhodium–hydroxybenzene complexes demonstrated that even noncoordinating counterions can elicit substantial changes in both the frequency and intensity of phenolic O–H stretches in charged species dissolved in organic solvents.³⁵ It is important to emphasize that in our system, once a suitable intramolecular hydrogen bond acceptor is present, the resulting spectra are well resolved. The key N–H stretches agree across all experimental methods and align nicely with theoretical values.

¹⁹F NMR Analysis. NMR spectroscopy is a powerful technique for evaluating hydrogen bonding between a variety of nuclei³⁶ because analysis of spin–spin coupling constants can validate the presence of many hydrogen bonds. Table 1 demonstrates the relationship between predicted hydrogen bond length and the couplings associated with various NH–F interactions.³⁷ In our estimation, the sharing of electron density through the hydrogen bond should lead to a significant NH–F coupling that may correlate to its strength.

Table 1. A Brief Survey of Selected NH–F Contacts

| fluoroamine | coupling constants ^a | | bond length, F–H _{in} ^b |
|-------------|---------------------------------|------------------------------|---|
| | $J_{\text{FH}_{\text{in}}}$ | $J_{\text{FH}_{\text{out}}}$ | |
| | 11.7 | 5.0 | 1.99 |
| | 12.7(11.5) | 4.1(2.5) | 1.99 |
| | 44.3(43.7) | - | 1.78 |

^a Absolute values of predicted constants, in hertz (Hz). Experimental values in parentheses. ^b Predicted, in angstroms (Å).

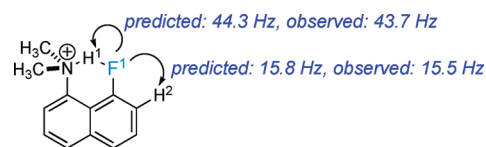


Figure 20. Major coupling constants; predicted vs observed.

When BARF salt **16** was dissolved in dichloromethane-*d*₂ at room temperature, we observed a resolved multiplet centered at −122.0 ppm that featured two major couplings of 43.7 and 15.5 Hz, as well as smaller, minor couplings (<2 Hz). The substantial 43.7 Hz coupling is too large to be caused by long-range, through-bond coupling, but can be explained by significant, direct overlap of a filled fluorine *n* orbital with an empty σ^* orbital of the charged donor (Figure 2). A 15.5 Hz constant is consistent with fluorine coupling to the ortho hydrogen, while smaller couplings are typical of normal long-range F–H interactions within the fluoronaphthalene system. In addition, geometry optimization and coupling constant calculations performed at the DFT/B3LYP/6-311++G** level predict major couplings of 44.3 and 15.8 Hz (F1···H1 and F1···H2, respectively, Figure 20). Because of this substantial coupling between the ammonium hydrogen and naphthalene fluorine, it is highly likely that the hydrogen bonding partners are within close proximity, presumably in the realm of the 1.78 Å predicted by theory (Table 1).

Because hydrogen bonds can be susceptible to intermolecular forces, we expected our system to be perturbed by solvent effects and counterion coordination. By simply switching the counterion from BARF to triflate and chloride, we noticed significant changes in the fluorine chemical shift and the NH–F coupling patterns (Table 2). The chloride ion appeared to suppress any resolved coupling, and a large, broad peak was detected at −108.1 ppm. The triflate ion appeared less coordinating and provided a broad doublet at −117.5 ppm. On the basis of these observations, the BARF salt was reanalyzed. Changing the solvent from dichloromethane to the hydrogen-bond-accepting acetonitrile produced a single broad peak at −115.2 ppm with no definable coupling pattern. It is clear that a significant NH–F interaction occurs and that the manifestation of defined coupling

Table 2. Summary of ^{19}F NMR Studies

| counterion | solvent | δ , F ^a | multiplicity ^b | coupling ^c |
|-----------------|--------------------------|---------------------------|---------------------------|-----------------------|
| Cl^- | CD_2Cl_2 | -108.1 | bs | — |
| TfO^- | CD_2Cl_2 | -117.5 | bd | 11.2 |
| BARF^- | CD_2Cl_2 | -122.0 | m | 43.7, 15.5, <2.0 |
| BARF^- | CD_3CN | -115.2 | bs | — |

^a In ppm, relative to CFCl_3 . ^b bs, broad singlet; bd, broad doublet; m, multiplet. ^c In hertz.

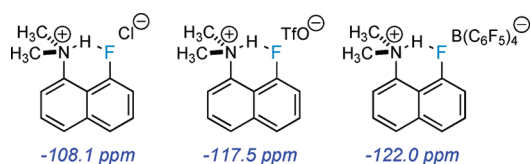


Figure 21. Counterion effect on the chemical shift of the naphthyl fluorine in CD_2Cl_2 .

patterns is highly dependent on the nature of the counterion and solvent utilized.

The observed trend in chemical shift is consistent with an accumulation of electron density³⁸ on fluorine that accompanies an increasing degree of hydrogen bonding between the ammonium ion donor and fluorine acceptor; stronger intramolecular interactions are possible as the solvent and counterion become less coordinating. In the progression from chloride to BARF, the naphthyl fluorine demonstrates a pronounced upfield shift of 13.9 ppm in CD_2Cl_2 (Figure 21). As intramolecular hydrogen bonding intensifies, the key fluorine experiences increased shielding and the chemical shift becomes more negative. When the solvent is changed from dichloromethane to acetonitrile, the hydrogen bond in the BARF species is partially disrupted. Comparatively less electron density resides on the naphthyl fluorine, and the corresponding chemical shift moves downfield by nearly 7 ppm. These results also demonstrate the presence of an intramolecular $\text{NH}\cdots\text{F}$ hydrogen bond and are summarized in Table 2.

CONCLUSIONS

Intramolecular hydrogen bonding between a charged NH donor and covalently bound organic fluorine acceptor has been thoroughly demonstrated through a variety of methods. Independently, each experiment provides detailed insight into the nature of the hydrogen bonding interaction. More importantly, the results as a whole are consistent unto themselves; congruous evidence for charged $\text{NH}\cdots\text{F}$ hydrogen bonding is provided in solution and in the solid state and is isolated in the gas phase, where all results agree with computation. All together, these results validate the physical–chemical role that charged hydrogen bonding to covalent fluorine may play in biological systems.

EXPERIMENTAL SECTION

General Methods. Unless otherwise stated, all reactions were performed under strictly anhydrous conditions under dry nitrogen or argon gas. Solvents were dried and purified by standard techniques. ^1H , ^{13}C , and ^{19}F NMR spectra were acquired on 300, 400, and 500 MHz instruments in CD_3CN , CD_2Cl_2 , or CDCl_3 at room temperature (25 °C). The chemical shifts are given in parts per million (δ) with

respect to internal tetramethylsilane, fluorotrichloromethane, or residual solvent peaks. NMR data is reported in the following format: chemical shift, multiplicity (singlet, s; doublet, d; triplet, t; multiplet, m; broad singlet, bs; broad doublet, bd), integration, coupling constant (Hz). FTIR spectra were recorded using a standard NaCl or CaF_2 cells. Melting points are uncorrected. In addition, compounds **4**³⁹ and **6**⁴⁰ were prepared according to literature procedures.

8-Fluoro-*N,N*-dimethylnaphthalen-1-amine (1). A mixture of 3 M sulfuric acid (3.50 mL, 10.5 mmol) and 37% aqueous formaldehyde (2.15 mL, 26.5 mmol) was cooled with stirring at 0 °C. A slurry of 1-amino-8-fluoronaphthalene³⁹ (1.00 g, 12.41 mmol) and sodium borohydride (1.12 g, 43.4 mmol) was added, and the mixture was stirred for 1 h. After completion of the reaction, solid sodium hydroxide was added to basify the solution. The oily supernatant was isolated and saved. The remaining aqueous solution was diluted with water (20 mL) and extracted with ether (2 × 20 mL). The organic solutions were combined, washed with saturated sodium chloride solution (20 mL), and dried with magnesium sulfate. The mix was filtered through celite, and the solvent was removed under reduced pressure. The crude product was purified by silica gel flash column chromatography with hexanes to yield a clear liquid that solidified upon cooling to give white crystals that melted slightly above room temperature (0.939 g, 80% yield); mp = 28–30 °C; ^1H NMR (CDCl_3) (25 °C) δ 7.59 (d, 1H), δ 7.52–7.31 (m, 3H), δ 7.14–7.01 (m, 2H), δ 2.87 (m, 6H); ^{13}C NMR (CDCl_3) δ 160.0, 149.6, 137.5, 126.5 (d, J = 1.5 Hz), 125.6 (d, J = 9.3 Hz), 124.5 (d, J = 4.4 Hz), 121.8, 118.9, 113.9, 111.1 (d, J = 25.0 Hz), 45.3, 45.2; ^{19}F NMR (CDCl_3) δ -112.7 (d, J = 15.1 Hz); IR 2949, 2734, 2790, 1591, 1383, 1023 (cm^{-1} , CaF_2 , CH_2Cl_2); HRMS (ESI+) calcd for $\text{C}_{12}\text{H}_{12}\text{FNNa}^+$: 212.08483, found 212.08362.

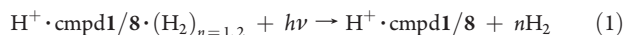
4-Fluoro-*N,N*-dimethylnaphthalen-1-amine (7). A mixture of 3 M sulfuric acid (2.25 mL, 6.75 mmol) and 37% aqueous formaldehyde (1.38 mL, 17.0 mmol) was cooled with stirring at 0 °C. A slurry of 1-amino-4-fluoronaphthalene¹⁷ (0.643 g, 7.98 mmol) and sodium borohydride (0.720 g, 27.9 mmol) was added, and the mixture was stirred for 1 h. After completion of the reaction, solid sodium hydroxide was added to basify the solution. The oily supernatant was isolated and saved. The remaining aqueous solution was diluted with water (20 mL) and extracted with ether (2 × 20 mL). The organic solutions were combined, washed with saturated sodium chloride solution (20 mL), and dried with magnesium sulfate. The mix was filtered through celite, and the solvent was removed under reduced pressure. The crude product was purified by silica gel flash column chromatography with hexanes to yield a tan oil (0.604 g, 82% yield). ^1H NMR (CDCl_3) (25 °C) δ 8.25 (m, 1H), δ 8.08 (m, 1H), δ 7.56–7.52 (m, 2H), δ 7.05 (t, 1H), δ 7.03–6.98 (m, 1H), δ 2.86 (s, 6H); ^{13}C NMR (CDCl_3) δ 156.2, 153.8, 147.1 (d, J = 3.6 Hz), 130.0 (d, J = 4.4 Hz), 126.0, 124.6 (d, J = 17.4 Hz), 124.1 (d, J = 2.8 Hz), 120.9 (d, J = 5.2 Hz), 113.5 (d, J = 8.1 Hz), 108.7 (d, J = 20.5 Hz), 45.4; ^{19}F NMR (CDCl_3) δ -130.4, bs; IR 2945, 2733, 2789, 1601, 1393, 1057 (cm^{-1} , CaF_2 , CH_2Cl_2); HRMS (ESI+) calcd for $\text{C}_{12}\text{H}_{12}\text{FNNa}^+$: 212.08483, found 212.08373.

Potentiometric Titrations. Potentiometric titrations of **1**, **7**, and **8** were carried out with a standard glass electrode and a pH meter, utilizing procedures similar to those developed by Chatten^{21a} and Streuli.²² Nitromethane was thoroughly dried (CaH_2) and distilled immediately before use. Perchloric acid titrant (0.1M) was prepared from standard 70% perchloric acid, and solutions of the analytes were prepared in nitromethane containing 0.2 mequiv per 50 mL solution. Titrations of each analyte were conducted in triplicate. Data points were collected at 0.1 mL titrant intervals, with reduction to 0.05 mL intervals surrounding the predicted inflection point. A third-order polynomial fit was obtained for the 20–80% neutralization region in each data set. By removing the first and fifth quintiles, a moderate reduction in the error of the fit was achieved. Upon double differentiation of the resulting third-order fitting functions, solving for the zero yielded the inflection point.

Following interpolation of this value upon the fitting function and correction for the offset of the titration probe, the $E_{1/2}$ (half neutralization potential, HNP) for each data set was determined. Further details are contained within the Supporting Information

Cryogenic Ion Photofragmentation Spectrometer. The Yale time-of-flight photofragmentation mass spectrometer used to carry out H_2/D_2 photodissociation has been previously described in detail.⁴¹ In brief, ~ 1 mM solutions of protonated **1** and **8** were generated by dissolving the appropriate amount of either compound in a mixture of $\sim 1\%$ 2 M aqueous formic acid in HPLC grade acetonitrile. The resulting solutions were electrosprayed through a PicoTip emitter (15 μ m diameter, NewObjective) by applying 1.5–2.5 kV. Electrosprayed ions were injected into the mass spectrometer through a stainless steel capillary that was maintained at a temperature of ~ 80 °C. RF-only ion guides were used to propagate the ions through four differentially pumped regions (1, 0.2, 10^{-4} , 10^{-7} torr), and prior to entering the quadrupole ion trap (Jordan TOF Products, Inc.), ions were turned 90° by a DC quadrupole. The ion trap was cooled to ~ 10 K using a closed cycle He cryostat (Sumitomo), where an 80:20 He: $H_2(D_2)$ buffer gas mixture was introduced into the ion trap through a pulsed valve (Parker Hannifin, Series 99, 1 ms pulse, 10 psi backing pressure). Ions were stored in the ~ 10 K ion trap between 70 and 90 ms, where they were trapped and cooled through collisions with the buffer gas, and $H_2(D_2)$ was condensed onto the ion of interest. The weakly bound adducts were then extracted from the trap by applying voltage pulses of opposite polarity to the entrance and exit trap electrodes, propelling them into the first stage of a TOF spectrometer where they were separated using standard time-of-flight techniques.

Tunable infrared radiation in the 2600–3600 cm^{-1} energy range was generated using an OPO/OPA (LaserVision) system that was pumped by a Nd:YAG (10 Hz, 7 ns). The 800–2500 cm^{-1} energy range was accessed by additional mixing of the OPA outputs in a AgGaSe2 crystal. While the vibrational spectrum of protonated **1** was collected throughout this region, the resulting spectra had poor signal-to-noise. Fortunately the diagnostic N–H stretch does not fall in this region. The isolated ion packet was intersected with the laser at the Wiley–McLaren temporal focus, and resonant absorption of a single photon resulted in the dissociation of the adduct via eq 1:



A vibrational spectrum was generated by plotting the fragment ion intensity as a function of photon energy. Laser power was adjusted to ensure that spectra were collected in the linear action regime, and spectra were normalized with respect to laser power to account for deviations in power across the photon energy range.

Computational Methods. Calculations were performed with Spartan '06 or the Gaussian 09 package.⁴² Unless specifically stated otherwise, geometry optimizations and vibrational analyses for the solution IR studies were carried out using the B3LYP functional at the 6-311+G** level of theory and scaled⁴³ by 0.986. Coupling constants were computed using the DFT/B3LYP functional at the 6-311+G** level of theory. In addition, the Gaussian 09 package was used to calculate minimum energy structures and harmonic frequency calculations of protonated compounds **1** and **8** at the MP2/6-311+G** level of theory. In this case, harmonic frequency calculations were scaled by 0.943, a value that brings the calculated N–H stretch into agreement with the experimental measure value for protonated compound **8**. This scaling factor falls within one standard deviation of the value listed on the NIST Webbook for the given method.⁴⁴

Preparation of Ammonium Salts. Ammonium chloride salts were prepared by protonation/deuteration of the corresponding *N,N*-dimethylamino-1-naphthalene precursor with HCl/DCl (g). HCl (g) and DCl (g) were dried with Drierite followed by passage through concentrated sulfuric acid (98% H_2SO_4 or 98% D_2SO_4). The dried gas

was then bubbled through a solution of the appropriate *N,N*-dimethylamino-1-naphthalene compound in dichloromethane until TLC of the reaction showed complete consumption of starting material. The solvent was removed in vacuo and the resulting salt was utilized immediately. Ammonium triflate salts were prepared by treatment of a cooled (-78 °C) solution of the appropriate *N,N*-dimethylamino-1-naphthalene in dichloromethane with 1.0 equiv of triflic acid (HOTf/DOTf) in dichloromethane. The reactions were stirred under nitrogen and allowed to warm to room temperature until TLC of the reaction showed complete consumption of starting material. The solvents were removed in vacuo, and the resulting salt was utilized immediately.

Method for BARF Ion Exchange. The appropriate ammonium chloride was dissolved in dichloromethane. Solid potassium tetrakis-(2,3,4,5,6-pentafluorophenyl) borate (K-BARF) (1.0 equiv) was added to the solution in one portion under a stream of nitrogen, and the mixture was allowed to stir at room temperature for 1 h. The resulting inorganic salts were removed by filtration through Chromafil O-20/25 Teflon syringe filters (0.2 μ m). The resulting solution was evaporated under vacuum to yield crystals of the desired BARF salt which was used immediately.

X-ray Crystallography. X-ray quality crystals of **15** and **16** were grown by the vapor diffusion method. The target salt was placed in a small vial and dissolved in dichloromethane. The vial was placed in a larger vial filled with a small amount of hexanes. The larger outer vial was capped, and the entire setup was stored under nitrogen, in the dark, in a desiccator until crystal growth was complete.

All reflection intensities were measured at 110(2) K with enhance graphite-monochromated Mo K α radiation ($\lambda = 0.71073$ Å) under the program CrysAlisPro (Version 1.171.33.55, Oxford Diffraction Ltd., 2010). The program CrysAlisPro (Version 1.171.33.55, Oxford Diffraction Ltd., 2010) was used to refine the cell dimensions. Data reduction was done using the program CrysAlisPro (Version 1.171.33.55, Oxford Diffraction Ltd., 2010). The structure was solved with the program SHELXS-97 (Sheldrick, 2008) and was refined on F^2 with SHELXL-97.⁴⁵ Analytical numeric absorption corrections based on a multifaceted crystal model were applied using CrysAlisPro (Version 1.171.33.55, Oxford Diffraction Ltd., 2010). The temperature of the data collection was controlled using the system Cryojet. The H-atoms (except for H1) were placed at calculated positions using the instructions AFIX 43 or AFIX 137 with isotropic displacement parameters having values 1.2 or 1.5 times U_{eq} of the attached C atoms. The coordinates and the isotropic temperature factor for the H1 atom (attached to N1) were refined freely.

NMR Spectroscopy Coupling Experiments. ¹⁹F NMR experiments for the coupling constant determinations were conducted on a 500 MHz NMR spectrometer at room temperature in dichloromethane- d_2 or acetonitrile- d_3 with trace $CFCl_3$ as a standard. Each substrate was dissolved in the desired solvent under nitrogen and syringed into an NMR tube fitted with a septum and maintained under a nitrogen atmosphere.

■ ASSOCIATED CONTENT

Supporting Information. NMR spectra, titration data, solution IR spectra, X-ray parameters. This material is available free of charge via the Internet at <http://pubs.acs.org>.

■ AUTHOR INFORMATION

Corresponding Author

*E-mail: mark_johnson@yale.edu; lectka@jhu.edu.

■ ACKNOWLEDGMENT

The authors thank Professor Kenneth Karlin for a gift of K-BARF, Professor Gerald Meyer for the use of his FT-IR spectrometer and Professor Howard Fairbrother for the use of

his pH probe. We also thank Dr. Ananya Majumdar for assistance with the NMR coupling experiments. T.L. thanks the John Simon Guggenheim Memorial Foundation, and M.A.J. thanks the NSF under grant CHE-091199 and the Air Force Office of Scientific Research under grant FA-9550-09-1-0139 for the development of the cryogenic ESI spectrometer.

REFERENCES

- (1) Jeffrey, G. A.; Saenger, W. *Hydrogen Bonding in Biological Structures*; Springer-Verlag: Berlin, 1991.
- (2) Carosati, E.; Simone, S.; Cruciani, G. *J. Med. Chem.* **2004**, *47*, 5114–5125.
- (3) Urzhumtsev, A.; Tête-Favier, F.; Mitschler, A.; Barbanton, J.; Barth, P.; Urzhumtseva, L.; Biellmann, J.-F.; Podjarny, A. D.; Moras, D. *Structure* **1997**, *5*, 601–612.
- (4) White, A.; Tull, D.; Johns, K.; Withers, S. G.; Rose, D. *Nat. Struct. Biol.* **1996**, *3*, 149–154.
- (5) Bystrom, C. E.; Pettigrew, D. W.; Branchaud, B. P.; O'Brien, P.; Remington, S. J. *Biochemistry* **1999**, *38*, 3508–3518.
- (6) Davis, A. M.; Teague, S. J. *Angew. Chem., Int. Ed.* **1999**, *38*, 736–749.
- (7) Takahashi, L. H.; Radhakrishnan, R.; Rosenfield, R. E., Jr.; Meyer, E. F., Jr.; Trainor, D. A. *J. Am. Chem. Soc.* **1989**, *111*, 3368–3374.
- (8) Istvan, E.; Deisenhofer, J. *Science* **2001**, *292*, 1160–1164.
- (9) Sidhu, G.; Withers, S. G.; Nguyen, N. T.; McIntosh, L. P.; Ziser, L.; Brayer, G. D. *Biochemistry* **1999**, *38*, 5346–5354.
- (10) Gonin, P.; Xu, Y.; Milon, L.; Dabernat, S.; Morr, M.; Kumar, R.; Lacombe, M. L.; Janin, J.; Lascu, I. *Biochemistry* **1999**, *38*, 7256–7272.
- (11) (a) Takemura, H.; Uesa, R.; Iwanaga, T. *J. Fluorine Chem.* **2009**, *130*, 684–688. (b) Takemura, H.; Kotoku, M.; Yasutake, M.; Shinmyozu, T. *Eur. J. Org. Chem.* **2004**, *9*, 2019–2024. (c) Biamonte, M. A.; Vasella, A. *Helv. Chim. Acta* **1998**, *81*, 695–717.
- (12) (a) Pham, M.; Gdaniec, M.; Polonski, T. *J. Org. Chem.* **1998**, *63*, 3731–3734. (b) Jakobsche, C. E.; Peris, G.; Miller, S. J. *Angew. Chem., Int. Ed.* **2008**, *47*, 6707–6711. (c) Golubev, N. S.; Shenderovich, I. G.; Smirnov, S. N.; Denisov, G. S.; Limbach, H. H. *Chem. Eur. J.* **1999**, *5*, 492–497. (d) Hennig, L.; Ayala-Leon, K.; Angulo-Cornejo, J.; Richter, R.; Beyer, L. J. *Fluorine Chem.* **2009**, *130*, 453–460. (e) Fritz, H.; Winkler, T. *Helv. Chim. Acta* **1974**, *57*, 836–839. (f) Fritz, H.; Winkler, T.; Küng, W. *Helv. Chim. Acta* **1975**, *58*, 1822–1824. (g) Rae, I. D.; Weigold, J. A.; Contreras, R. H.; Biekofsky, R. R. *Magn. Reson. Chem.* **1993**, *31*, 836–840.
- (13) (a) Cox, C.; Wack, H.; Lectka, T. *Angew. Chem., Int. Ed.* **1999**, *38*, 798–800. (b) Ozeryanskii, V. A.; Pozharskii, A. F.; Bienko, A. J.; Sawka-Dobrowolska, W.; Sobczyk, L. *J. Phys. Chem. A* **2005**, *109*, 1637–1642. (c) Llamas-Siaz, A. L.; Foces-Foces, C.; Elguero, J. *J. Mol. Struct.* **1994**, *328*, 297–323. (d) Ozeryanskii, V. A.; Pozharskii, A. F.; Glowiak, T.; Majerz, I.; Sobczyk, L.; Grech, E.; Nowicka-Scheibe, J. *J. Mol. Struct.* **2002**, *607*, 1–8. (e) Perrin, C. L.; Ohta, B. K. *J. Am. Chem. Soc.* **2001**, *123*, 6520–6526. (f) Perrin, C. L.; Ohta, B. K. *J. Mol. Struct.* **2003**, *644*, 1–12.
- (14) Zhu, Z.; Colbry, N. L.; Lovadahl, M.; Mennen, K. E.; Acciacca, A.; Beylin, V. G.; Clark, J. D.; Belmont, D. T. *Org. Prep. Process Res. Dev.* **2007**, *11*, 907–909.
- (15) Giumanini, A. G.; Chiavari, G.; Musiani, M. M.; Rossi, P. *Synthesis* **1980**, *9*, 743–746.
- (16) Lammers, J. G.; Cornelisse, J. *Isr. J. Chem.* **1977**, *16*, 299–303.
- (17) Adcock, W.; Dewar, M. J. S. *J. Am. Chem. Soc.* **1967**, *89*, 386–390.
- (18) Carey, F. A.; Sundberg, R. J. *Advanced Organic Chemistry, Fourth Edition, Part A; Structure and Mechanisms*; Springer Science+Business Media, Inc.: New York, 2000.
- (19) Bondi, A. *J. Phys. Chem.* **1964**, *68*, 441–451.
- (20) Bortoluzzi, M.; Annibale, G.; Paolucci, G.; Pitteri, B. *Polyhedron* **2008**, *27*, 1497–1502.
- (21) (a) Chatten, L. G.; Harris, L. E. *Anal. Chem.* **1962**, *34*, 1495–1501. (b) Hall, H. K. *J. Phys. Chem.* **1956**, *60*, 63–70.
- (22) Streuli, C. A. *Anal. Chem.* **1959**, *31*, 1652–1654.
- (23) (a) Liao, M. S.; Watts, J. D.; Gorun, S. M.; Scheiner, S.; Huang, M. J. *J. Theor. Comput. Chem.* **2008**, *7*, 541–563. (b) Scheiner, S.; Kar, T. *J. Phys. Chem. A* **2008**, *112*, 11854–11860. (c) Scheiner, S. *J. Phys. Chem. B* **2009**, *113*, 10421–10427. (d) Solimannejad, M.; Scheiner, S. *J. Phys. Chem. A* **2007**, *111*, 4431–4435. (e) Scheiner, S.; Kar, T. *J. Mol. Struct.* **2007**, *844–845*, 166–172.
- (24) Howard, S. *J. Am. Chem. Soc.* **2000**, *122*, 8238–8244.
- (25) (a) Bartoszak-Adamska, E.; Jaskólski, M.; Brzezinski, B. *J. Mol. Struct.* **1998**, *448*, 57–62. (b) Desiraju, G. R. *Acc. Chem. Res.* **1991**, *24*, 290–296. (c) Desiraju, G. R. *Acc. Chem. Res.* **1996**, *29*, 441–449.
- (26) (a) Bacchi, A.; Bosetti, E.; Carcelli, M.; Pelagatti, P.; Rogolino, D. *Eur. J. Inorg. Chem.* **2004**, 1985–1991. (b) Zhang, J.; Ren, H.; Liu, L. *Chem. Lett.* **2010**, *39*, 1016–1017.
- (27) Tetrakis(2,3,4,5,6-pentafluorophenyl) borate, $B(C_6F_5)_4^{1-}$.
- (28) Pimentel, G. C.; McClellan, A. L. *The Hydrogen Bond*; W. H. Freeman and Company: San Francisco, 1960.
- (29) (a) Wozniak, K.; Krygowski, T. M.; Pawlak, D.; Kolodziejski, W.; Grech, E. *J. Phys. Org. Chem.* **1997**, *10*, 814–824. (b) Mallinson, P. R.; Smith, G. T.; Wilson, C. C.; Grech, E.; Wozniak, K. *J. Am. Chem. Soc.* **2003**, *125*, 4259–4270. (c) Mallinson, P. R.; Wozniak, K.; Wilson, C. C.; McCormack, K. L.; Yufit, D. S. *J. Am. Chem. Soc.* **1999**, *121*, 4640–4646.
- (30) Steiner, T. *J. Chem. Soc., Perkin Trans. 2* **1995**, 1315–1319.
- (31) Silverstein, R. M.; Webster, F. X.; Kiemle, D. J. *Spectroscopic Identification of Organic Compounds*, 7th ed.; John Wiley & Sons: Hoboken, 2005; pp 76–77.
- (32) (a) Rabasco, J. J.; Kass, S. R. *J. Am. Soc. Mass. Spectrom.* **1992**, *3*, 91–98. (b) Baschky, M. C.; Peterson, K. C.; Kass, S. R. *J. Am. Chem. Soc.* **1994**, *116*, 7218–7224. (c) Reed, D. R.; Kass, S. R.; Mondanaro, K. R.; Dailey, W. P. *J. Am. Chem. Soc.* **2002**, *124*, 2790–2795. (d) Tian, Z.; Kass, S. R. *Annu. Rep. Prog. Chem., Sect. B* **2006**, *102*, 290–324. (e) Tian, Z.; Lis, L.; Kass, S. R. *J. Am. Chem. Soc.* **2008**, *130*, 8–9. (f) Kong, J.; Mayer, P. S.; Morton, T. H. *Int. J. Mass Spectrom.* **2002**, *217*, 257–271. (g) Leblanc, D.; Kong, J.; Mayer, P. S.; Morton, T. H. *Int. J. Mass Spectrom.* **2003**, *222*, 451–463. (h) Nguyen, V.; Mayer, P. S.; Morton, T. H. *J. Org. Chem.* **2000**, *65*, 8032–8040. (i) Kohler, B. E.; Morton, T. H.; Nguyen, V.; Shaler, T. A. *J. Phys. Chem. A* **1999**, *103*, 2302–2309. (j) Shaler, T. A.; Morton, T. H. *J. Am. Chem. Soc.* **1994**, *116*, 9222–9226. (k) Nguyen, V.; Cheng, X.; Morton, T. H. *J. Am. Chem. Soc.* **1992**, *114*, 7127–7132. (l) O'Brien, J. T.; Prell, J. S.; Berden, G.; Oomens, J.; Williams, E. R. *Int. J. Mass Spectrom.* **2010**, *297*, 116–123. (m) Prell, J. S.; O'Brien, J. T.; Steill, J. D.; Oomens, J.; Williams, E. R. *J. Am. Chem. Soc.* **2009**, *131*, 11442–11449. (n) Forbes, M. W.; Bush, M. F.; Polfer, N. C.; Oomens, J.; Dunbar, R. C.; Williams, R. C.; Jockusch, R. A. *J. Phys. Chem. A* **2007**, *111*, 11759–11770. (o) Kamarriotis, A.; Boyarkin, O. V.; Mercier, S. R.; Beck, R. D.; Bush, M. F.; Williams, E. R.; Rizzo, T. R. *J. Am. Chem. Soc.* **2006**, *128*, 905–916.
- (33) (a) Stearns, J. A.; Boyarkin, O. V.; Rizzo, T. R. *J. Am. Chem. Soc.* **2007**, *129*, 13820–13821. (b) Goebbert, D. J.; Wende, T.; Bergmann, R.; Meijer, G.; Asmis, K. R. *J. Phys. Chem. A* **2009**, *113*, 5874–5880. (c) Kamrath, M. Z.; Garand, E.; Jordan, P. A.; Leavitt, C. M.; Wolk, A. B.; Van Stipdonk, M. J.; Miller, S. J.; Johnson, M. A. *J. Am. Chem. Soc.* **2011**, *133*, 6440–6448.
- (34) Rospenk, M.; Zeegers-Huyskens, T. *J. Phys. Chem.* **1987**, *91*, 3974–3977.
- (35) Son, S. U.; Reingold, J. A.; Carpenter, G. B.; Czech, P. T.; Sweigart, D. A. *Organometallics* **2006**, *25*, 5276–5285.
- (36) (a) Pietrzak, M.; Try, A. C.; Andrioletti, B.; Sessler, J. L.; Anzenbacher, P., Jr.; Limbach, H. H. *Angew. Chem., Int. Ed.* **2008**, *47*, 1123–1126. (b) Wasylshen, R.; Schaefer, T. *Can. J. Chem.* **1970**, *48*, 1263–1268. (c) Del Bene, J. E.; Ajith Perera, S.; Bartlett, R. J. *J. Am. Chem. Soc.* **2000**, *122*, 3560–3561. (d) Pecul, M.; Sadlej, J.; Leszczynski, J. *J. Chem. Phys.* **2001**, *115*, 5498–5506. (e) Afonin, A. V.; Ushakov, I. A.; Mikhaleva, A. I.; Trofimov, B. A. *Magn. Reson. Chem.* **2007**, *45*, 220–230. (f) Blake, P. R.; Park, J. B.; Adams, M. W. W.; Summers, M. F. *J. Am. Chem. Soc.* **1992**, *114*, 4931–4933. (g) Shenderovich, I. G.; Tolstoy, P. M.; Golubev, N. S.; Smirnov, S. N.; Denisov, G. S.; Limbach, H. H. *J. Am. Chem. Soc.* **2003**, *125*, 11710–11720.

(37) (a) Alkorta, I.; Elguero, J.; Limbach, H. H.; Shenderovich, I.; Winkler, T. *Magn. Reson. Chem.* **2009**, *47*, 585–592. (b) Fritz, H.; Winkler, T.; Küng, W. *Helv. Chim. Acta* **1975**, *58*, 1822–1824. (c) Rae, I. D.; Weigold, J. A.; Contreras, R. H.; Biekofsky, R. R. *Magn. Reson. Chem.* **1993**, *31*, 836–840.

(38) It is known that the electron density of the donor and acceptor atoms increase during hydrogen bonding: Del Bene, J. E.; Elguero, J. *J. Am. Chem. Soc.* **2004**, *126*, 15624–15631.

(39) Zhu, Z.; Colbry, N. L.; Lovdahl, M.; Mennen, K. E.; Acciacca, A.; Beylin, V. G.; Clark, J. D.; Belmont, D. T. *Org. Prep. Process Res. Dev.* **2007**, *11*, 907–909.

(40) Lammers, J. G.; Cornelisse, J. *Isr. J. Chem.* **1977**, *16*, 299–303.

(41) (a) Kamrath, M. Z.; Relph, R. A.; Guasco, T. L.; Leavitt, C. M.; Johnson, M. A. *Int. J. Mass Spectrom.* **2010**, *300*, 91–98. (b) Johnson, M. A.; Lineberger, W. C. Pulsed Methods for Cluster Ion Spectroscopy. In *Techniques for the Study of Ion Molecule Reactions*; Farrar, J. M., Saunders, W. H., Jr., Eds.; Wiley: New York, 1988; Vol. XX; p 591.

(42) Frisch, M. J.; Trucks, G. W.; Schlegel, H. B.; Scuseria, G. E.; Robb, M. A.; Cheeseman, J. R.; Scalmani, G.; Barone, V.; Mennucci, B.; Petersson, G. A.; Nakatsuji, H.; Caricato, M.; Li, X.; Hratchian, H. P.; Izmaylov, A. F.; Bloino, J.; Zheng, G.; Sonnenberg, J. L.; Hada, M.; Ehara, M.; Toyota, K.; Fukuda, R.; Hasegawa, J.; Ishida, M.; Nakajima, T.; Honda, Y.; Kitao, O.; Nakai, H.; Vreven, T.; Montgomery, J. A., Jr.; Peralta, J. E.; Ogliaro, F.; Bearpark, M.; Heyd, J. J.; Brothers, E.; Kudin, K. N.; Staroverov, V. N.; Kobayashi, R.; Normand, J.; Raghavachari, K.; Rendell, A.; Burant, J. C.; Iyengar, S. S.; Tomasi, J.; Cossi, M.; Rega, N.; Millam, N. J.; Klene, M.; Knox, J. E.; Cross, J. B.; Bakken, V.; Adamo, C.; Jaramillo, J.; Gomperts, R.; Stratmann, R. E.; Yazyev, O.; Austin, A. J.; Cammi, R.; Pomelli, C.; Ochterski, J. W.; Martin, R. L.; Morokuma, K.; Zakrzewski, V. G.; Voth, G. A.; Salvador, P.; Dannenberg, J. J.; Dapprich, S.; Daniels, A. D.; Farkas, Ö.; Foresman, J. B.; Ortiz, J. V.; Cioslowski, J.; Fox, D. J. *Gaussian 09, Revision A. 02*, Gaussian, Inc., Wallingford, CT, 2009.

(43) Merrick, J. P.; Moran, D.; Radom, L. *J. Phys. Chem. A* **2007**, *111*, 11683–11700.

(44) NIST Computational Chemistry Comparison and Benchmark Database, N. S. R. D. N., Release 15a, April 2010; Johnson R. D., III, Ed.; <http://cccbdb.nist.gov/>.

(45) Sheldrick, G. M. *Acta Crystallogr., Sect. A: Found. Crystallogr.* **2008**, *64*, 112–122.